RSC Advances

PAPER

View Article Online
View Journal | View Issue

Cite this: *RSC Adv.*, 2015, **5**, 29456

Design, synthesis and biological evaluation of novel C3-functionalized oxindoles as potential Pim-1 kinase inhibitors

Hong-bao Sun,†[a] Xiao-yan Wang,†[b] Guo-bo Li,[a] Li-dan Zhang,[c] Jie Liu*[a] and Li-feng Zhao*[a]

A novel series of C3-functionalized oxindoles, 3-(2-oxo-4-phenylbut-3-en-1-ylidene)indolin-2-ones, were designed, synthesized and investigated for inhibition of cell proliferation against different types of human cancer cell lines, including SW620, HeLa and A549. This biological study showed that these compounds containing the scaffolds of indole and aromatic α,β-unsaturated ketone had moderate to significant antitumor activities. Further study suggested that compound **4b**, as one of this kind of structure derivative, showed broad-spectrum antitumor activities against MCF-7, PC-3, SKOV-3, U87, SMMC-7721, SY5Y and A875 cancer cell lines. Besides, the results of the inhibition of Pim kinases indicated that compound **4b** showed selective and efficient anti-Pim-1 kinase activity (IC_{50} = 5 μM). Docking simulation, flow cytometry (FCM), and Hoechst 33342 staining assay suggested that the most active compound **4b** induced cell death through apoptosis *via* binding to the active ATP pocket of Pim-1. Moreover, it showed that compound **4b** had strong inhibition of tubulin polymerization which may be caused by inhibiting Pim-1.

Received 5th January 2015
Accepted 12th March 2015

DOI: 10.1039/c5ra00177c

www.rsc.org/advances

Introduction

Pim-1, a member of the Pim kinases family (Pim-1, Pim-2 and Pim-3), is a serine/threonine protein kinase identified by cloning the retroviral integration sites in Moloney *murine leukemia virus* induced lymphomas. Pim-1 has been implicated to function in several normal biological process including cell cycle regulation, cell survival, proliferation and differentiation. It can phosphorylate Cdc25A and Cdc25C to enhance G_1/S transition and G_2/M transition, respectively.[1,2] The phosphorylation of the pro-apoptotic protein Bad at Ser112 induced by Pim-1 blocks apoptotic cell death.[3] Pim-1 also inactivates ASK1 through phosphorylation at Ser83 leading to less caspase3 activation and reducing cell death.[4] Moreover, Pim-1 associates with tubulin and plays a vital role during mitosis.[5] However, when these processes become disrupted or hyper-activated, Pim-1 expresses several hallmarks of cancer. Numerous evidences confirmed Pim-1 kinase as a proto-oncogene. Pim-1 was found over-expression in many of human tumor diseases, such as hematologic malignancies,[6,7] bladder cancer,[8] prostate cancer,[9] gastric cancer.[10] Thus, inhibition of Pim-1 is considered as a valuable target for therapy of cancer.[11,12] It has attracted great interesting in developing novel inhibitors of Pim-1, and a large amount structurally different small molecule inhibitors have been obtained, such as SGI-1776,[13] SMI-4a,[14] DHPCC-9,[15] K00486,[16] CX-6258,[17] Cpd 14 (ref. 18) (Fig. 1). Despite these successes, only a few of them have been tested in cell-based assays or the related mechanisms of Pim kinases function to demonstrate anti-cancer activity. Only understanding the processes that can be targeted by Pim inhibition is of great importance for defining the potential activity of these compounds. Therefore, designing novel Pim-1 inhibitors that

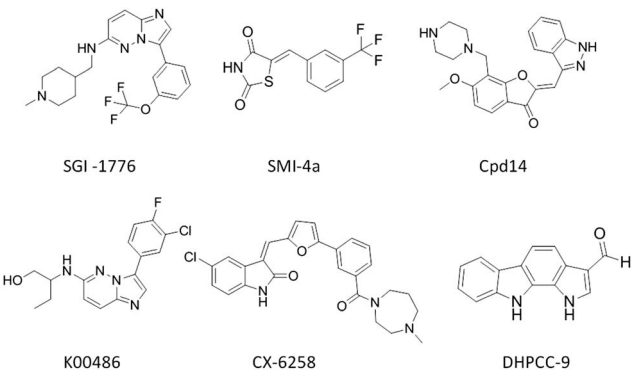

Fig. 1 Small molecule inhibitors targeting Pim family kinases.

[a]*State Key Laboratory of Biotherapy and Cancer Center, West China Hospital, Sichuan University, and Collaborative Innovation Center for Biotherapy, Chengdu 610041, China. E-mail: liujie2011@scu.edu.cn; lifengzhao@scu.edu.cn; Fax: +86-28-8550-3817; Tel: +86-28-8550-3817*

[b]*Analytical & Testing Center, Sichuan University, Chengdu 610064, China*

[c]*College of Chemical Engineering, Sichuan University, Chengdu 610064, China*

† These authors made equal contributions to this work.

targeted Pim and inhibited Pim kinases related function will still be a challenge for current anti-cancer drug discovery.

C3-functionalized oxindole is being continuously discovered to be at the core of several natural products, and becomes an emerging new scaffold for drug discovery with potential anti-cancer and other biological activities.[19–22] Among the representative examples are spiro-tetrahydrofuryl oxindole as anti-cancer agent,[23] spiro-isoxazolidinyl oxindole with anti-cancer and anti-tubercular activities,[24–26] pyrrolidinooxindole-type alkaloid CPC-1,[27] convolutamydine A with potent activity in the differentiation of HL-60 cells,[28] celogentin K as potential inhibitor of tubulin polymerization,[29] CX-6258 as Pim-1, 2, 3 inhibitor,[17] maremycins with anti-cancer activity[30] (Fig. 2). Another privileged skeletons, known chemically as chalcones, are biogenetic precursors of flavonoids in higher plants. These structures contain a ketone functionality and an unsaturated group (double bond), which are in conjugated arrangement among the naturally occurring or synthetic anti-cancer agents. The much flexible structure made it easier to combine with different protein receptors and exhibited good anti-canter activity (Fig. 2). Chalcone inhibited the proliferation of human breast cancer cell (MCF-7) by blocking cell cycle progression and inducing apoptosis.[31] Licochalcone A had excellent activities against MCF-7 and HL-60.[32] Isoliquiritigenin (ISL), isolated from Licorice, suppressed pulmonary metastasis of mouse renal cell carcinoma,[33] induced apoptosis and cell cycle arrest through p53 dependent pathway in HepG2.[34] The plant polyphenol butein, another nature product of derivative of chalcone, inhibited testosterone-induced proliferation in breast cancer cells expressing aromatase.[35] These privileged structures provide us new idea for designing novel drugs.

In the past decades, plentiful efforts have been started for treating a wide range and types of cancer, and chemotherapy had become a common treatment option for cancer patients.[36] One of well-known methods for primary anti-cancer drug discovery is combinatorial chemistry.[37] As it's a part of our own interest to develop some C3-functionalized oxindoles,[38] we conceived that combine C3-functionlized oxindoles with α,β-unsaturated ketones to obtain a novel series of compounds as potential Pim-1 inhibitors with great biological activities, as shown in Fig. 2. Based on our previous synthesis efforts,[39] herein we report the efficient synthesis of 3-(2-oxo-4-phenylbut-3-en-1-ylidene)indolin-2-ones with efficient and broad-spectrum anti-tumor activities *in vitro* and described the structure–activity relationship (SAR). The most effective compound **4b** was selected for further study. It showed selective and good inhibition against Pim-1 (IC_{50} = 5 μM). Docking simulation also suggested that Pim-1 is the potential target for compound **4b**. Further study, including flow cytometry (FCM), Hoechst 33342 staining assay and immunohistochemistry of tubulin indicated that compound **4b** caused cell arrest in G_2/M phase, induced cell apoptosis and had significant inhibition on tubulin polymerization, which may be all associated with the inhibition of Pim-1.

Result and discussion

The synthetic strategy to prepare the target compounds is depicted in Scheme 1. The key intermediates **3a–y** were prepared from benzylidene acetones and isatins as previously reported.[39] Then, targeted compounds **4a–y** were obtained, respectively, by the reaction with corresponding **3a–y** in the

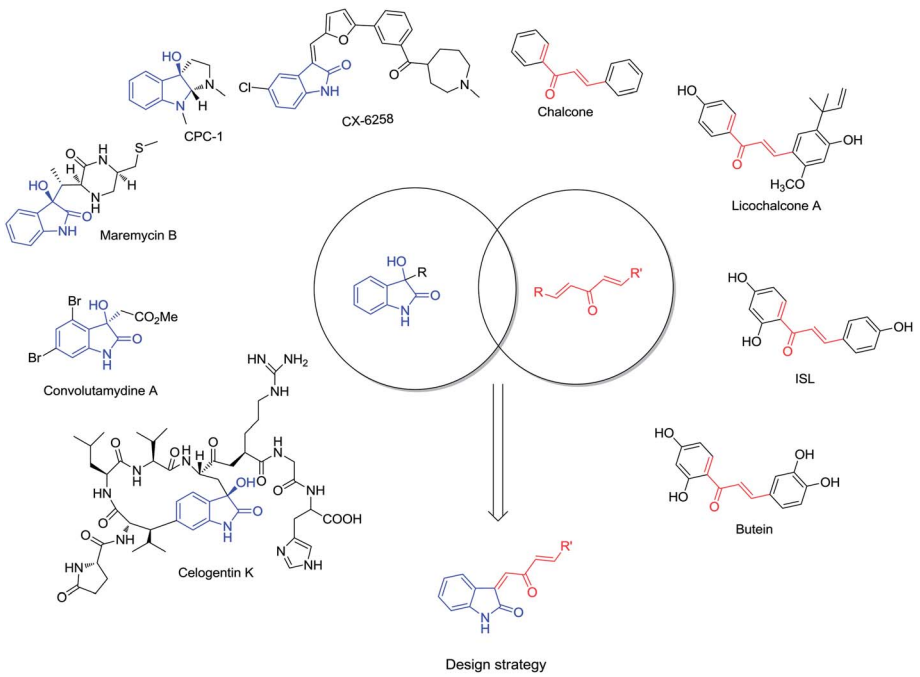

Fig. 2 Biologically important molecules containing C3-functionalized oxindoles or α,β-unsaturated ketones, and the design strategy of combinatorial chemistry for new compound.

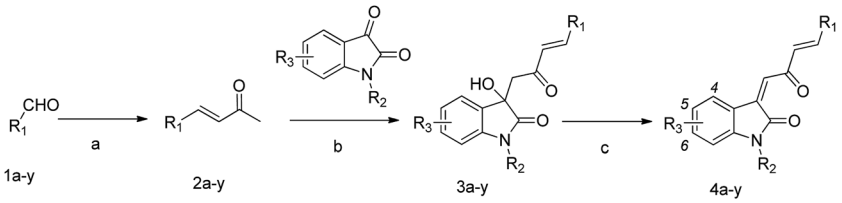

Scheme 1 Reagents and conditions: (a) CH_3COCH_3, H_2O, 0.5% NaOH, r. t, overnight; (b) 10% L-Arg, MeOH, r. t, overnight; (c) CCl_4, PPh_3, THF, reflux, overnight.

presence of CCl_4 and PPh_3 refluxing in THF, in moderate to high (up to 96%) yields. All the products were characterized by ^1H NMR, ^{13}C NMR, ^{19}F NMR and ESI-MS analysis.

All the newly synthesized compounds **4a–y** were investigated for their anti-proliferative activity on three human cancer cell lines including SW620, HeLa, and A549 *in vitro* by MTT assay method. The half maximal inhibitory concentrations (IC_{50}) of the tested compounds were listed in Table 1. These compounds exhibited good anti-tumor activities against SW620, and most of them had moderate to remarkable activities against A549. Their inhibitory effect on HeLa changed obviously with the different groups in the positions of R_1, R_2 and R_3. The structure–activity relationships (SAR) could be observed mainly related to the influence of various substituents in R_1, R_2 and R_3. The electronic properties and steric hindrance of the substituents at the aromatic ring had great influence on anti-tumor ability. The comparison of the activities of the pair of compounds **4b**/**4j** and **4c**/**4h**, the first of each pair component with a substituent at *para*-position (**4b** and **4c**) and the second with the corresponding substituent at *meta*-position (**4j**) or *ortho*-position (**4h**), showed that the compounds with substituents at *para*-position had higher activities (**4b**/**4j** IC_{50} = 1.53 and 6.72 μM, **4c**/**4h** IC_{50} = 2.20 and 2.96 μM, respectively). The activities of **4b**, **4c** and **4d** were 1.53 μM, 2.20 μM, and >20 μM, suggesting that the size of substituent at *para*-position had a huge influence on the activity, the bigger the substituent was, the lower the activity would be, and even lost activity. The IC_{50} of compound **4g** was 4.15 μM and **4d** was >20 μM, meaning that the activity changed little with the size of substituent at *meta*-position changing. Compounds **4q–t** and **4y** lost activities but compound **4p** had a good activity of 3.45 μM, indicating that R_1 group must be aromatic ring and there should be no substituent at the nitrogen.

To further study the anti-proliferative activity of this series of compounds, **4b**, **4c** and **4p** were selected for evaluation of their inhibitory activities against a panel of different types of human cancer cell lines: A549, HeLa, MCF-7, PC-3, SKOV-3, U87, SMMC-7721, SY5Y, A875. As shown in Table 2, generally speaking, all these compounds had much stronger inhibition activities than the positive control cisplatin. Compound **4b** (IC_{50} = 1.53 μM, 0.47 μM, 4.67 μM, 3.29 μM and 1.13 μM for HeLa, PC-3, U87, SMMC-7721 and SY5Y, respectively) showed the best anti-proliferative activities against the cancer cell lines of HeLa, PC-3, U87, SMMC-7721 and SY5Y. Meanwhile, compound **4p** (IC_{50} = 3.21 μM, 4.02 μM, 2.2 μM and 0.22 μM against A549, MCF-7, skov-3 and A875, respectively) had most effective activities on A549, MCF-7, skov-3 and A875 cell lines. It indicated that these compounds had broad-spectrum anti-proliferative activity against human cancers.

At the beginning of design these compounds, our project was to develop new Pim-1 inhibitors as anti-tumor agents. Therefore we performed kinase assay to examine whether the compounds

Table 1 *In vitro* activities of compounds **4a–y**

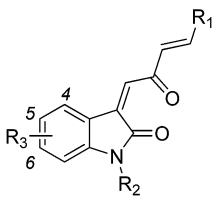

Compound	R_1	R_2	R_3	IC_{50}[a] (μM) SW620	HeLa	A549
4a	Ph	H	H	0.19	3.18	5.03
4b	4-F–C_6H_4	H	H	0.13	1.53	2.02
4c	4-Cl–C_6H_4	H	H	1.68	2.20	3.86
4d	4-Br–C_6H_4	H	H	1.97	>20	15.41
4e	4-$CH(CH_3)_2$–C_6H_4	H	H	1.56	2.64	3.97
4f	4-MeO–C_6H_4	H	H	1.98	8.46	17.32
4g	3-Br–C_6H_4	H	H	1.34	3.15	7.31
4h	3-Cl–C_6H_4	H	H	1.21	2.96	3.01
4i	3-CF_3–C_6H_4	H	H	0.57	6.13	3.15
4j	2-F–C_6H_4	H	H	0.46	6.72	5.58
4k	3,4-DiCl–C_6H_4	H	H	0.49	>20	8.86
4l	3,4-DiMe–C_6H_4	H	H	0.76	2.43	10.21
4m	2,4-DiCl–C_6H_4	H	H	0.54	>20	4.34
4n	2-F–4-Br–C_6H_4	H	H	2.31	>20	>20
4o	2,3,4-TriMeO–C_6H_4	H	H	0.91	>20	4.95
4p	2-Naphthyl	H	H	0.28	3.45	2.57
4q	2-Furyl	H	H	2.03	>20	3.85
4r	2-Thienyl	H	H	2.54	>20	4.92
4s	Cyclohexyl	H	H	3.21	>20	10.22
4t	$CH(CH_3)_2$	H	H	3.87	>20	>20
4u	Ph	H	4-Cl	0.67	7.96	7.81
4v	Ph	H	6-Cl	0.35	3.92	4.56
4w	Ph	H	5-Br	3.91	7.52	>20
4x	Ph	H	5-Me	0.03	>20	3.14
4y	Ph	Me	H	1.10	>20	5.50

[a] The anti-proliferation activities of compounds **4a–y** *in vitro* were determined by the MTT assay on Sw620, HeLa, A549 cell lines, IC50 was average of three determinations and deviation from the average was <5% of the average value.

Table 2 The anti-proliferation activities of compounds **4b**,**c**, **4p** and cisplatin against various cancer cell lines

	IC_{50}[a] (μM)								
Compound	A549	HeLa	MCF-7	PC-3	SKOV-3	U87	SMMC-7721	SY5Y	A875
4b	3.53	1.53	4.86	0.47	2.39	4.67	3.29	1.13	1.03
4c	4.74	2.2	10.93	3.28	3.22	9.94	6.84	1.74	1.78
4p	3.21	3.45	4.02	2.47	2.2	9.08	4.32	1.16	0.22
Cisplatin[b]	10.05	5.02	>20	10	5.25	11.08	6.35	1.71	4.15

[a] Values were average of three determinations and deviation from the average is <5% of the average value. [b] Positive control.

(**4b**, **4c**, **4p**) interact with Pim kinases and inhibit Pim kinases, *in vitro*. Compound **4b** (IC_{50} = 5 μM) showed more effective than compound **4c** (IC_{50} = 7 μM) and **4p** (IC_{50} = 10 μM) against Pim-1. In addition, the IC_{50} of compound **4b** against Pim-1, -2, and -3 were 5 μM, >20 μM and 15 μM, respectively. It suggested that compound **4b** had selective and good inhibition against Pim-1.

Based on these results, compound **4b** was selected as a lead compound for further study because of its best potency against most of the cancer cells and selective inhibition of Pim-1, *in vitro*. For better understanding of the potency of compound **4b** and guiding further SAR studies, we evaluated the interaction between compound **4b** and Pim kinases (Pim-1, Pim-2 and Pim-3). The compound **4b** bound to the active site of ATP and the binding modes of compound **4b** to Pim kinases were exhibited in Fig. 3. Firstly, we used molecular docking to analyze the binding mode of compound **4b** with Pim-1. A total of 20 docking poses were generated by GOLD program. According to the RMSD values, two docking pose clusters (cluster I and cluster II) were obtained. Cluster I contained 16 docking poses, while cluster II only had 4 docking poses. Therefore, we considered that the docking poses in cluster I might be the true binding modes of compound **4b** with Pim-1. Fig. 3a depicted the binding pose of compound **4b** with the highest Goldscore value of 48.231. The amide group of compound **4b** was observed to form strong hydrogen-bonding interactions with Lys67 and Glu89. The fluorine atom of compound **4b** formed halogen-bonding interaction with Leu44. In addition, compound **4b** formed intensive hydrophobic interactions with residues Leu93, Leu120, Leu44, Val52, Lys67 and Ile185. The interaction mode between compound **4b** and Pim-1 was corresponded to the SAR. Then, we analyzed the binding modes of compound **4b** with Pim-2 and Pim-3. The results showed that the compound **4b** did not perfectly match with Pim-2 and Pim-3, comparing with Pim-1 (see Fig. 3b and c). Goldscore for the compound **4b** binding with Pim-2 and Pim-3 were 45.241 and 41.398, respectively, which slightly lower than that with Pim-1. These results may be used for explaining why the inhibitory activity of compound **4b** against Pim-1 was better than Pim-2 and Pim-3. Finally, we also further predicted the other possible kinase targets for compound **4b** using a reverse molecule docking method.[40] The top 10 kinases ranked by the reverse molecule docking method were AKT-1, BCR-ABL, CLK3, KIT, CK2, MAPK14, PEPCK, ALK5, CaMKK2, TGFR1, respectively. These kinases may be the targets of compound **4b**.

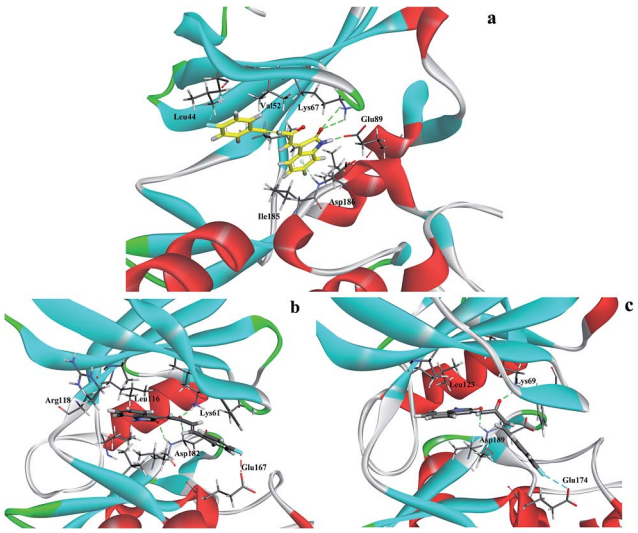

Fig. 3 Molecular docking compound **4b** with Pim kinases (a) binding mode of compound **4b** (represented with stick) to the ATP binding pocket of Pim-1 (PDB ID: 1XWS). (b) Binding mode of compound **4b** (represented with stick) to the ATP binding pocket of Pim-2. (c) Binding mode of compound **4b** (represented with stick) to the ATP binding pocket of Pim-3.

Next, compound **4b** was used to evaluate other biological functions associated with Pim-1. Flow cytometric analysis was used to quantitatively assess and the cell cycle after PI-stained. As shown in Fig. 4a significant accumulation of cells in the S phase, accompanied by a decrease in G_0/G_1 phase was observed after treatment with compound **4b** in HeLa cancer cells at 1 μM. However a large amount of tetraploid and polyploidies were appeared in contrast with a sharply decreasing cells in G_0/G_1 phase and S phase from 2 μM to 3 μM. The results suggested that compound **4b** arrested the cell divided during the DNA replicating. In addition, fluorescence microscopic examination of Hoechst 33342 stained cell confirmed the inducing apoptosis effect of compound **4b**. The apoptotic cells are often characterized by its morphological, including cell shrinkage, membrane blabbing, chromatin condensation and DNA fragmentation. After treated with compound **4b** for 48 hours, HeLa cells shrank and rounded up. With the increasing of concentration, it became more significant. In contrast, the untreated HeLa cells retained their normal size and shape, kept proliferating with time and became over-crowded by 36 hours (Fig. 5A). Morphological changes were also characteristic of apoptosis after Hoechst 33342 staining. Apoptosis cells, bright blue

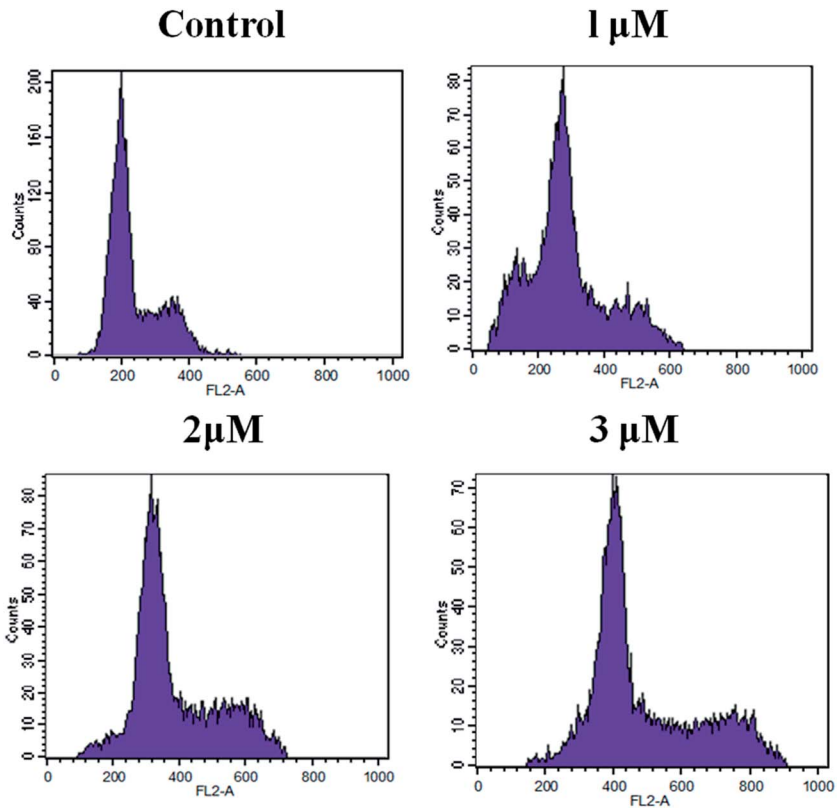

Fig. 4 Effect of compound **4b** on cell cycle distribution: DNA fluorescence histograms of PI-stained HeLa cells. Cells were treated with 1 μM, 2 μM, 3 μM for 48 h.

fluorescent and condensed nuclei, were observed in a large number of treated cells in HeLa, and the change was concentration-dependent, whereas there was no significant apoptosis in untreated HeLa cells that showed blue, diffusely stained intact nuclei (Fig. 5B). These results suggested that compound **4b** induced apoptosis in HeLa cells.

To further test the apoptosis inducing ability of **4b**, an Annexin-V/PI fluorescence staining was analyzed by flow cytometry in HeLa cells. As shown in Fig. 6, HeLa cells were treated with **4b** at the concentrations of 0, 2, 4 and 8 μM for 48 h. We found an obvious concentration-dependent reduction in the percentage of surviving cells. As the concentration of compound **4b** increased, the early and the late stage apoptotic cells increased from 9.04% at 2 μM to 62.31% at 8 μM. This result indicated that compound **4b** induced apoptosis of HeLa cells in a dose-dependent manner.

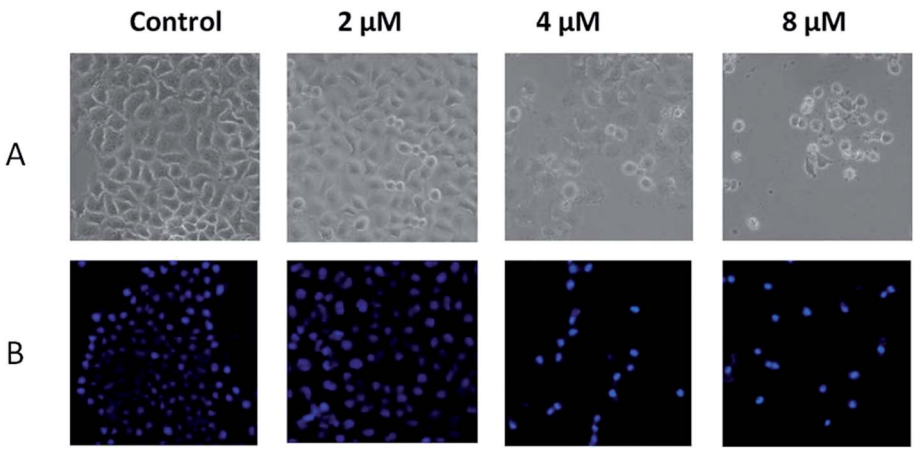

Fig. 5 Effect of compound **4b** on cell morphology: (A) bright-field microscopy images and (B) fluorescence microscopic appearance of Hoechst 33342 staining nuclei of HeLa cells, after incubation with compound **4b** for 48 h at varying concentrations: 2 μM, 4 μM, 8 μM. Apoptosis cells were observed in treated cells containing condensed and fragmented fluorescent nuclei.

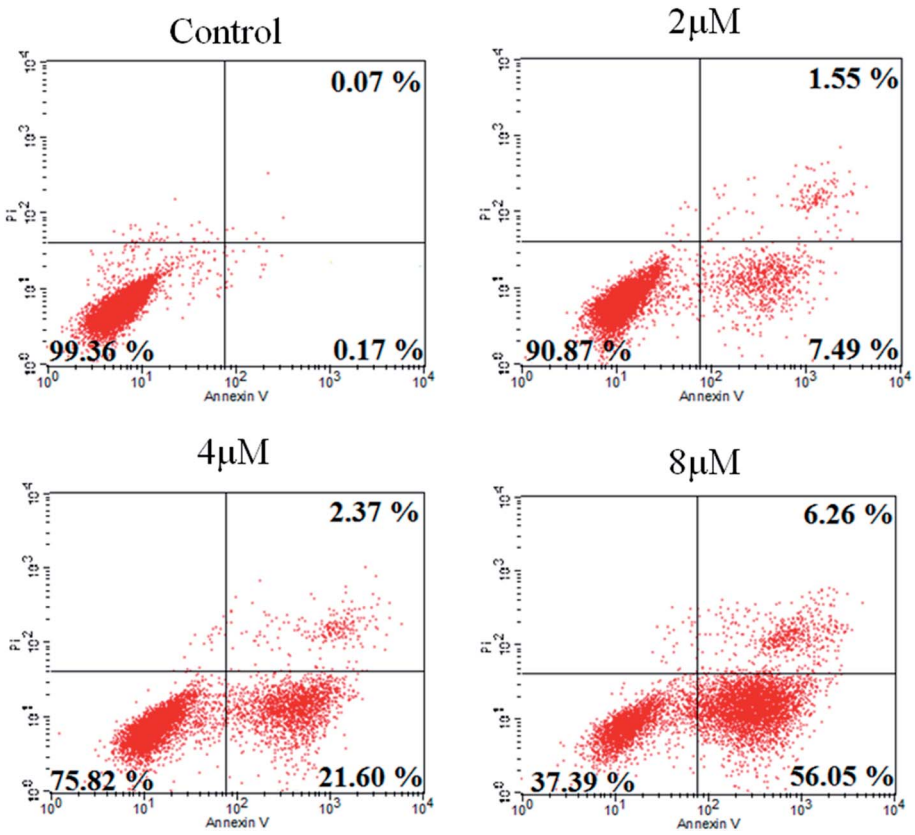

Fig. 6 Compound **4b** induces apoptosis in HeLa cells. Flow cytometric analysis of cells stained with Annexin V-FITC/PI after treatment with various concentrations (0 μM, 2 μM, 4 μM and 8 μM) of compound **4b** for 48 hours.

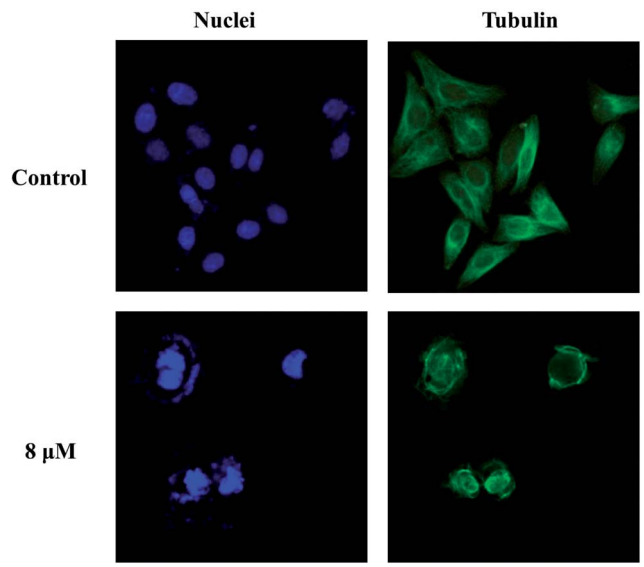

Fig. 7 HeLa cells were treated with compounds **4b** with 8 μM for 24 h followed by staining with α-tubulin antibody. Chromosomal DNA (blue) was stained with DAPI. Microtubule organization was clearly observed by green tubulin network-like structures in control cells, and was found to be disrupted in cells treated with compound **4b**.

We also validated the effect of compound **4b** on cellular tubulin immunohistochemistry. Studies were carried out to examine the *in situ* effects of compound **4b** on cellular microtubules in HeLa cells. HeLa cells seeded on sterile cover slips were treated with compound **4b** at 2 μM for 48 h. As shown in Fig. 7, untreated HeLa cells displayed the normal distribution of microtubules. However, cells treated with compound **4b** showed disrupted microtubule organization, thus demonstrated the inhibition of tubulin polymerization, influenced the mitosis and affected the cell division in an orderly and programmed manner. This process may be all associated with the inhibition of Pim-1. In dividing cells, Pim-1 is located in the mitotic spindle and specifically the spindle poles, which plays the key role of influencing the function of mitotic spindle.[5] When Pim-1 was inhibited by compound **4b**, the function of spindle was disturbed and then the microtubule constituted spindle fibers was disorder just as observed in Fig. 7. Finally the cells were arrested in G_2/M phase and apoptosis. The result also explained the appearance of polyploidy in flow cytometric analysis.

Experimental

Materials and measurements

Melting points were recorded at SGW X-4 Melting point instrument (Shanghai precision & scientific instrument Co., Ltd, Shanghai, China). ^{1}H NMR spectra were recorded at 400

MHz. The chemical shifts were recorded in ppm relative to tetramethylsilane and with the solvent resonance as the internal standard. Data were reported as follows: chemical shift, multiplicity (s = singlet, d = doublet, t = triplet, q = quartet, m = multiplet), coupling constants (Hz), integration. ^{13}C NMR data were collected at 100 MHz with complete proton decoupling. Chemical shifts were reported in ppm from the tetramethylsilane with the solvent resonance as internal standard. ^{19}F NMR data were collected at 376 MHz with complete proton decoupling. ESI-HRMS spectra were recorded on a commercial apparatus and methanol was used to dissolve the sample. All chemicals were obtained from commercial sources and used without further purification. Column chromatography was carried out on silica gel (300–400 mesh, Qingdao Marine Chemical Ltd, Qingdao, China). Thin layer chromatography (TLC) was performed on TLC silica gel 60 F254 plates.

General procedure for the synthesis of benzylidene acetones (2a–t)

To a stirred solution of **1a–t** (10 mmol) in 2 mL acetone and 1 mL H_2O was added 0.25 mL 10% NaOH aqua and stirred at room temperature for 12 hours. Then the solvent was removed under reduced pressure and the residue was extracted with acetic ether. The combined organic layers were dried ($MgSO_4$), filtered and the filtrate was concentrated under reduced pressure. The crude product was used for next step.

General procedure for the synthesis of 3-hydroxy-3-(2-oxo-4-phenylbut-3-en-1-yl)indolin-2-ones (3a–y)

A mixture of isatin (0.1 mmol), (*E*)-4-phenylbut-3-en-2-one (**2a**, 0.1 mmol), arginine (0.01 mmol) in MeOH (1.0 mL) was stirred for 48 hours at 25 °C. After completion of the reaction (TLC), the solvent was removed under vacuum. The crude product was subjected to column chromatography on silica gel using petroleum ether/ethyl acetate = 1 : 1 as the eluent to give **3a**.

Compounds **3b–y** were synthesized by a similar procedure as described for compound **3a**. For the separation of these compounds, the eluent of silica gel column chromatography consisted of appropriate mixtures of petroleum ether and ethyl acetate.

General procedure for the synthesis of 3-(2-oxo-4-phenylbut-3-en-1-ylidene)indolin-2-ones (4a–y)

Compound **3a–y** (0.2 mmol) was dissolved in anhydrous THF (4 mL). Ph_3P (78.7 mg, 0.3 mmol) and CCl_4 (0.1 mL) were then added. The solution was heated to reflux for 12 hours. After completion of the reaction (TLC), the solvent was removed under vacuum. The crude product was subjected to column chromatography on silica gel using petroleum ether/ethyl acetate = 2 : 1 as the eluent to give **4a–y**.

(*Z*)-3-((*E*)-2-Oxo-4-phenylbut-3-en-1-ylidene)indolin-2-one (4a)

Red solid, yield 89%, m. p. 176–177 °C; ^{1}H-NMR (400 MHz, DMSO) δ 10.78 (s, 1H), 8.29 (d, J = 8.0 Hz, 1H), 7.74 (dd, J = 10.0, 6.0 Hz, 3H), 7.44–7.38 (m, 4H), 7.32 (dd, J = 21.2, 12.0 Hz, 2H), 6.97 (t, J = 7.6 Hz, 1H), 6.88 (d, J = 7.6 Hz, 1H); ^{13}C-NMR (100 MHz, DMSO) δ 190.1, 168.6, 144.8, 144.6, 136.0, 134.1, 133.1, 131.1, 129.1, 128.8, 127.80, 127.5, 127.2, 121.8, 120.1, 110.3; ESI-MS: m/z 274.1 $[M - H]^-$.

(*Z*)-3-((*E*)-4-(4-Fluorophenyl)-2-oxobut-3-en-1-ylidene)indolin-2-one (4b)

Red solid, yield 96%, m. p. 204–205 °C; ^{1}H-NMR (400 MHz, DMSO) δ 10.77 (s, 1H), 8.36 (d, J = 8.0 Hz, 1H), 7.90 (dd, J = 8.4, 6.0 Hz, 2H), 7.79 (d, J = 16.0 Hz, 1H), 7.42–7.26 (m, 5H), 6.99 (t, J = 8.0 Hz, 1H), 6.88 (d, J = 8.0 Hz, 1H); ^{13}C-NMR (100 MHz, DMSO) δ 189.9, 168.5, 163.6 (d, J = 248 Hz), 145.0, 143.2, 136.2, 133.1, 131.3 (d, J = 8.6 Hz), 131.0 (d, J = 2.9 Hz), 127.8, 127.7 (d, J = 2.3 Hz), 127.4, 121.7, 120.3, 116.1 (d, J = 21.8 Hz), 110.3; ^{19}F-NMR (376 MHz, DMSO) δ −108.9; ESI-MS: m/z 292.1 $[M - H]^-$.

(*Z*)-3-((*E*)-4-(4-Chlorophenyl)-2-oxobut-3-en-1-ylidene)indolin-2-one (4c)

Red solid, yield 93%, m. p. 215–216 °C; ^{1}H-NMR (400 MHz, DMSO) δ 10.78 (s, 1H), 8.38 (d, J = 7.6 Hz, 1H), 7.86 (d, J = 8.4 Hz, 2H), 7.78 (d, J = 16.0 Hz, 1H), 7.53 (d, J = 8.4 Hz, 2H), 7.45–7.35 (m, 3H), 7.00 (t, J = 7.6 Hz, 1H), 6.88 (d, J = 7.6 Hz, 1H); ^{13}C-NMR (100 MHz, DMSO) δ 189.8, 168.4, 145.1, 142.9, 136.3, 135.5, 133.3, 133.2, 130.6, 129.1, 128.4, 127.6, 127.4, 121.7, 120.2, 110.3; ESI-MS: m/z 308.2 $[M - H]^-$.

(*Z*)-3-((*E*)-4-(4-Bromophenyl)-2-oxobut-3-en-1-ylidene)indolin-2-one (4d)

Red solid, yield 92%, m. p. 222–223 °C; ^{1}H-NMR (400 MHz, DMSO) δ 10.78 (s, 1H), 8.38 (d, J = 7.6 Hz, 1H), 7.78 (dd, J = 12.4, 8.0 Hz, 3H), 7.67 (d, J = 8.4 Hz, 2H), 7.48–7.33 (m, 3H), 7.00 (t, J = 7.6 Hz, 1H), 6.88 (d, J = 7.6 Hz, 1H); ^{13}C-NMR (100 MHz, DMSO) δ 189.81, 168.4, 145.1, 143.0, 136.3, 133.6, 133.2, 132.0, 130.8, 128.4, 127.6, 127.4, 124.4, 121.7, 120.2, 110.3; ESI-MS: m/z 352.2 $[M - H]^-$.

(*Z*)-3-((*E*)-4-(4-Isopropylphenyl)-2-oxobut-3-en-1-ylidene) indolin-2-one (4e)

Red solid, yield 91%, m. p. 184–185 °C; ^{1}H-NMR (400 MHz, DMSO) δ 10.77 (s, 1H), 8.37 (d, J = 7.6 Hz, 1H), 7.76 (dd, J = 12.0, 10.4 Hz, 3H), 7.42 (s, 1H), 7.39–7.27 (m, 4H), 6.99 (t, J = 7.6 Hz, 1H), 6.89 (d, J = 7.6 Hz, 1H), 2.92 (m, 1H), 1.22 (d, J = 6.8 Hz, 6H); ^{13}C-NMR (100 MHz, DMSO) δ 189.9, 168.5, 151.9, 145.0, 144.5, 136.0, 133.0, 132.0, 129.1, 127.9, 127.3, 127.0, 126.9, 121.7, 120.3, 110.2, 33.4, 23.5; ESI-MS: m/z 316.1 $[M - H]^-$.

(*Z*)-3-((*E*)-4-(4-Methoxyphenyl)-2-oxobut-3-en-1-ylidene) indolin-2-one (4f)

Red solid, yield 65%, m. p. 180–181 °C; ^{1}H-NMR (400 MHz, DMSO) δ 10.76 (s, 1H), 8.36 (d, J = 7.6 Hz, 1H), 7.84–7.72 (m, 3H), 7.40–7.33 (m, 2H), 7.27 (d, J = 16.0 Hz, 1H), 7.06–6.95 (m, 3H), 6.88 (d, J = 7.6 Hz, 1H), 3.83 (s, 3H); ^{13}C-NMR (100 MHz, DMSO) δ 189.7, 168.5, 161.7, 144.9, 144.6, 135.7, 132.9, 130.9, 128.2, 127.3, 126.8, 125.4, 121.7, 120.3, 114.6, 110.2, 55.4; ESI-MS: m/z 304.0 $[M - H]^-$.

(*Z*)-3-((*E*)-4-(3-Bromophenyl)-2-oxobut-3-en-1-ylidene)indolin-2-one (4g)

Red solid, yield 84%, m. p. 192–193 °C; ^{1}H-NMR (400 MHz, DMSO) δ 10.78 (s, 1H), 8.39 (d, J = 7.6 Hz, 1H), 8.10 (s, 1H), 7.83 (d, J = 7.6 Hz, 1H), 7.76 (d, J = 16.0 Hz, 1H), 7.65 (dd, J = 8.0, 0.8 Hz, 1H), 7.50 (d, J = 16.0 Hz, 1H), 7.46–7.34 (m, 3H), 7.00 (t, J = 7.6 Hz, 1H), 6.88 (d, J = 7.6 Hz, 1H); ^{13}C-NMR (100 MHz, DMSO) δ 189.8, 168.4, 145.1, 142.5, 136.9, 136.4, 133.33, 133.2, 131.2, 131.0, 129.1, 127.9, 127.6, 127.4, 122.4, 121.7, 120.2, 110.3. ESI-MS: m/z 352.0 $[M - H]^-$.

(*Z*)-3-((*E*)-4-(3-Chlorophenyl)-2-oxobut-3-en-1-ylidene)indolin-2-one (4h)

Red solid, yield 83%, m. p. 192–193 °C; ^{1}H-NMR (400 MHz, DMSO) δ 10.77 (s, 1H), 8.39 (d, J = 7.6 Hz, 1H), 7.95 (s, 1H), 7.78 (dd, J = 11.6, 8.4 Hz, 2H), 7.58–7.44 (m, 3H), 7.44–7.30 (m, 2H), 7.00 (t, J = 7.6 Hz, 1H), 6.89 (d, J = 7.6 Hz, 1H); ^{13}C-NMR (100 MHz, DMSO) δ 189.8, 168.4, 145.1, 142.5, 136.6, 136.4, 133.8, 133.2, 130.8, 130.4, 129.1, 128.3, 127.5, 127.5, 127.4, 121.7, 120.2, 110.3; ESI-MS: m/z 308.1 $[M - H]^-$.

(*Z*)-3-((*E*)-2-Oxo-4-(3-(trifluoromethyl)phenyl)but-3-en-1-ylidene)indolin-2-one (4i)

Red solid, yield 79%, m. p. 178–179 °C; ^{1}H-NMR (400 MHz, DMSO) δ 10.79 (s, 1H), 8.32 (d, J = 7.6 Hz, 1H), 8.15 (s, 1H), 8.06 (d, J = 7.6 Hz, 1H), 7.84–7.76 (m, 2H), 7.66 (t, J = 7.6 Hz, 1H), 7.48 (d, J = 16.0 Hz, 1H), 7.41–7.29 (m, 2H), 6.97 (dd, J = 11.2, 4.4 Hz, 1H), 6.88 (d, J = 7.6 Hz, 1H); ^{13}C-NMR (100 MHz, DMSO) δ 190.0, 168.6, 144.9, 142.5, 136.4, 135.3, 133.3, 132.4, 130.1, 130.0, 129.3, 127.5, 127.3, 127.1 (q, J = 6.3 Hz), 125.3 (q, J = 7.4 Hz), 121.9, 120.1, 110.4, 48.6; ^{19}F-NMR (376 MHz, DMSO) δ −61.2; ESI-MS: m/z 342.1 $[M - H]^-$.

(*Z*)-3-((*E*)-4-(2-Fluorophenyl)-2-oxobut-3-en-1-ylidene)indolin-2-one (4j)

Red solid, yield 94%, m. p. 186–187 °C; ^{1}H-NMR (400 MHz, DMSO) δ 10.79 (s, 1H), 8.32 (d, J = 7.6 Hz, 1H), 7.88 (t, J = 7.6 Hz, 1H), 7.76 (d, J = 16.0 Hz, 1H), 7.59–7.17 (m, 6H), 6.97 (t, J = 7.6 Hz, 1H), 6.87 (d, J = 7.6 Hz, 1H); ^{13}C-NMR (100 MHz, DMSO) δ 189.7, 168.6, 160.9 (d, J = 250.6 Hz), 144.9, 136.4, 135.8 (d, J = 3.3 Hz), 133.3, 133.1 (d, J = 9.0 Hz), 129.4 (d, J = 4.8 Hz), 129.2 (d, J = 1.7 Hz), 127.5, 127.4, 125.1 (d, J = 3.1 Hz), 121.9, 121.8 (d, J = 11.2 Hz), 120.0, 116.1 (d, J = 21.4 Hz), 110.4; ^{19}F-NMR (376 MHz, DMSO) δ −115.4; ESI-MS: m/z 292.1 $[M - H]^-$.

(*Z*)-3-((*E*)-4-(3,4-Dichlorophenyl)-2-oxobut-3-en-1-ylidene)indolin-2-one (4k)

Red solid, yield 77%, m. p. 221–222 °C; ^{1}H-NMR (400 MHz, DMSO) δ 10.79 (s, 1H), 8.39 (d, J = 7.6 Hz, 1H), 8.17 (d, J = 2.0 Hz, 1H), 7.83 (dd, J = 8.4, 2.0 Hz, 1H), 7.75 (t, J = 12.4 Hz, 2H), 7.52 (d, J = 16.0 Hz, 1H), 7.43–7.34 (m, 2H), 7.00 (t, J = 7.6 Hz, 1H), 6.89 (d, J = 7.6 Hz, 1H); ^{13}C-NMR (100 MHz, DMSO) δ 189.7, 168.4, 145.1, 141.4, 136.5, 135.3, 133.3, 133.1, 131.8, 131.1, 130.5, 129.6, 128.8, 127.4, 127.4, 121.7, 120.2, 110.3; ESI-MS: m/z 342.1 $[M - H]^-$.

(*Z*)-3-((*E*)-4-(3,4-Dimethylphenyl)-2-oxobut-3-en-1-ylidene)indolin-2-one (4l)

Red solid, yield 74%, m. p. 198–199 °C; ^{1}H-NMR (400 MHz, DMSO) δ 10.76 (s, 1H), 8.36 (d, J = 7.6 Hz, 1H), 7.72 (d, J = 16.0 Hz, 1H), 7.61 (s, 1H), 7.53 (d, J = 7.6 Hz, 1H), 7.44–7.28 (m, 3H), 7.22 (d, J = 7.6 Hz, 1H), 6.99 (t, J = 7.6 Hz, 1H), 6.88 (d, J = 7.6 Hz, 1H), 2.26 (s, 6H); ^{13}C-NMR (100 MHz, DMSO) δ 189.7, 168.4, 144.9, 144.7, 140.1, 136.9, 135.9, 132.9, 131.9, 130.1, 129.8, 127.9, 127.3, 126.7, 126.6, 121.7, 120.3, 110.2, 19.5, 19.2; ESI-MS: m/z 302.1 $[M - H]^-$.

(*Z*)-3-((*E*)-4-(2,4-Dichlorophenyl)-2-oxobut-3-en-1-ylidene)indolin-2-one (4m)

Red solid, yield 78%, m. p. 214–215 °C; ^{1}H-NMR (400 MHz, DMSO) δ 10.80 (s, 1H), 8.45 (d, J = 7.6 Hz, 1H), 8.09 (d, J = 8.4 Hz, 1H), 7.93 (d, J = 16.0 Hz, 1H), 7.79 (d, J = 2.0 Hz, 1H), 7.66–7.51 (m, 2H), 7.43–7.33 (m, 2H), 7.01 (t, J = 7.6 Hz, 1H), 6.89 (d, J = 7.6 Hz, 1H); ^{13}C-NMR (100 MHz, DMSO) δ 189.4, 168.4, 145.2, 136.7, 134.4, 133.4, 130.6, 130.6, 130.2, 130.1, 128.4, 128.3, 127.5, 127.4, 121.8, 120.2, 119.8, 110.3; ESI-MS: m/z 342.0 $[M - H]^-$.

(*Z*)-3-((*E*)-4-(4-Bromo-2-fluorophenyl)-2-oxobut-3-en-1-ylidene)indolin-2-one (4n)

Red solid, yield 75%, m. p. 201–202 °C; ^{1}H-NMR (400 MHz, DMSO) δ 10.79 (s, 1H), 8.41 (d, J = 7.6 Hz, 1H), 7.93 (t, J = 8.0 Hz, 1H), 7.72 (dd, J = 12.4, 7.6 Hz, 2H), 7.53 (t, J = 12.8 Hz, 2H), 7.44–7.31 (m, 2H), 7.00 (t, J = 7.6 Hz, 1H), 6.88 (d, J = 7.6 Hz, 1H); ^{13}C-NMR (100 MHz, DMSO) δ 189.4, 168.4, 160.6 (d, J = 254.8 Hz), 145.2, 136.7, 134.4 (d, J = 2.5 Hz), 133.4, 130.6 (d, J = 2.6 Hz), 130.2 (d, J = 4.7 Hz), 128.4 (d, J = 3.0 Hz), 127.5, 127.4, 124.7 (d, J = 10.0 Hz) 121.8, 121.5 (d, J = 11.4 Hz), 120.2, 119.7 (d, J = 25.5 Hz), 110.3; ^{19}F-NMR (376 MHz, DMSO) δ −112.4; ESI-MS: m/z 370.1 $[M - H]^-$.

(*Z*)-3-((*E*)-2-Oxo-4-(2,3,4-trimethoxyphenyl)but-3-en-1-ylidene)indolin-2-one (4o)

Red solid, yield 75%, m. p. 178–179 °C; ^{1}H-NMR (400 MHz, DMSO) δ 10.78 (s, 1H), 8.31 (d, J = 7.6 Hz, 1H), 7.84 (d, J = 16.0 Hz, 1H), 7.60 (d, J = 8.8 Hz, 1H), 7.40–7.29 (m, 2H), 7.25 (d, J = 16.0 Hz, 1H), 6.98 (t, J = 7.6 Hz, 1H), 6.93–6.82 (m, 2H), 3.84 (s, 3H), 3.82 (s, 3H), 3.80 (s, 3H); ^{13}C-NMR (100 MHz, DMSO) δ 189.9, 168.7, 156.2, 153.2, 144.6, 141.7, 139.1, 135.7, 133.0, 128.4, 127.3, 125.9, 123.7, 121.9, 120.4, 120.1, 110.3, 108.6, 61.5, 60.5, 56.0; ESI-MS: m/z 364.1 $[M - H]^-$.

(*Z*)-3-((*E*)-4-(Naphthalen-2-yl)-2-oxobut-3-en-1-ylidene)indolin-2-one (4p)

Red solid, yield 93%, m. p. 199–200 °C; ^{1}H-NMR (400 MHz, DMSO) δ 10.80 (s, 1H), 8.33 (d, J = 7.6 Hz, 1H), 8.27 (s, 1H), 7.97–7.89 (m, 5H), 7.64–7.51 (m, 2H), 7.45 (d, J = 13.6 Hz, 2H), 7.35 (t, J = 7.6 Hz, 1H), 6.99 (t, J = 7.6 Hz, 1H), 6.89 (d, J = 7.6 Hz, 1H); ^{13}C-NMR (100 MHz, DMSO) δ 190.0, 168.6, 144.8, 144.7, 136.0, 134.0, 133.1, 132.8, 131.8, 131.2, 128.7, 128.6, 127.9, 127.8, 127.7, 127.4, 127.3, 126.9, 123.9, 121.9, 120.1, 110.4; ESI-MS: m/z 324.1 $[M - H]^-$.

(*Z*)-3-((*E*)-4-(Furan-2-yl)-2-oxobut-3-en-1-ylidene)indolin-2-one (4q)

Red solid, yield 88%, m. p. 184–185 °C; ^{1}H-NMR (400 MHz, DMSO) δ 10.76 (s, 1H), 8.29 (d, J = 6.0 Hz, 1H), 7.87 (s, 1H), 7.57 (d, J = 15.6 Hz, 1H), 7.32 (d, J = 6.8 Hz, 2H), 7.12–6.82 (m, 4H), 6.66 (s, 1H); ^{13}C-NMR (100 MHz, DMSO) δ 189.4, 168.6, 150.5, 146.8, 144.7, 135.9, 133.1, 130.9, 127.7, 127.3, 124.2, 121.8, 120.1, 118.3, 113.4, 110.3; ESI-MS: m/z 264.1$[M - H]^-$.

(*Z*)-3-((*E*)-2-Oxo-4-(thiophen-2-yl)but-3-en-1-ylidene)indolin-2-one (4r)

Red solid, yield 87%, m. p. 177–178 °C; ^{1}H-NMR (400 MHz, DMSO) δ 10.75 (s, 1H), 8.36 (d, J = 7.6 Hz, 1H), 7.98 (d, J = 15.6 Hz, 1H), 7.83 (d, J = 5.2 Hz, 1H), 7.68 (d, J = 3.6 Hz, 1H), 7.41–7.31 (m, 2H), 7.21 (dd, J = 4.8, 3.6 Hz, 1H), 7.04 (d, J = 15.8 Hz, 1H), 6.99 (t, J = 7.6 Hz, 1H), 6.88 (d, J = 7.6 Hz, 1H); ^{13}C-NMR (100 MHz, DMSO) δ 189.2, 168.5, 144.9, 139.4, 137.2, 135.9, 133.6, 133.0, 131.3, 128.9, 127.8, 127.4, 126.2, 121.7, 120.3, 110.2; ESI-MS: m/z 280.0 $[M - H]^-$.

(*Z*)-3-((*E*)-4-Cyclohexyl-2-oxobut-3-en-1-ylidene)indolin-2-one (4s)

Red solid, yield 73%, m. p. 196–197 °C; ^{1}H-NMR (400 MHz, DMSO) δ 11.21 (s, 1H), 7.55 (d, J = 7.6 Hz, 1H), 7.40 (s, 1H), 7.20 (t, J = 7.6 Hz, 1H), 7.03 (t, J = 7.6 Hz, 1H), 6.89 (d, J = 7.6 Hz, 1H), 6.27 (d, J = 12.0 Hz, 1H), 6.20 (d, J = 12.0 Hz, 1H), 2.31–2.21 (m, 1H), 1.65–1.47 (m, 4H), 1.36–1.07 (m, 6H); ^{13}C-NMR (100 MHz, DMSO) δ 189.9, 170.2, 150.7, 147.6, 140.0, 135.4, 128.3, 124.3, 122.5, 119.4, 118.1, 110.2, 37.4, 29.2, 28.38, 27.6, 26.8, 26.1; ESI-MS: m/z 280.1 $[M - H]^-$.

(*Z*)-3-((*E*)-5-Methyl-2-oxohex-3-en-1-ylidene)indolin-2-one (4t)

Red solid, yield 69%, m. p. 180–181 °C; ^{1}H-NMR (400 MHz, DMSO) δ 11.20 (s, 1H), 7.57 (d, J = 7.6 Hz, 1H), 7.40 (s, 1H), 7.19 (t, J = 7.6 Hz, 1H), 7.03 (t, J = 7.6 Hz, 1H), 6.89 (d, J = 7.6 Hz, 1H), 6.32 (d, J = 10.8 Hz, 1H), 6.14 (d, J = 12.0 Hz, 1H), 2.50 (m, 1H), 1.89 (s, 3H), 1.84 (s, 3H); ^{13}C-NMR (100 MHz, DMSO) δ 170.2, 150.3, 140.0, 139.5, 135.4, 128.3, 124.3, 122.63, 121.1, 119.5, 118.8, 110.2, 59.7, 26.6, 18.8; ESI-MS: m/z 240.2 $[M - H]^-$.

(*Z*)-4-Chloro-3-((*E*)-2-oxo-4-phenylbut-3-en-1-ylidene)indolin-2-one (4u)

Yellow solid, yield 95%, m. p. 217–218 °C; ^{1}H-NMR (400 MHz, DMSO) δ 10.90 (s, 1H), 7.80–7.69 (m, 3H), 7.57 (d, J = 16.4 Hz, 1H), 7.43 (dd, J = 5.2, 1.6 Hz, 3H), 7.32 (t, J = 8.0 Hz, 1H), 7.07 (t, J = 12.4 Hz, 2H), 6.86 (d, J = 7.6 Hz, 1H); ^{13}C-NMR (100 MHz, DMSO) δ 194.9, 165.7, 144.7, 144.2, 136.2, 134.3, 131.7, 130.7, 130.2, 129.2, 128.9, 128.6, 126.8, 122.7, 117.9, 109.0; ESI-MS: m/z 308.2 $[M - H]^-$.

(*Z*)-6-Chloro-3-((*E*)-2-oxo-4-phenylbut-3-en-1-ylidene)indolin-2-one (4v)

Red solid, yield 94%, m. p. 229–230 °C; ^{1}H-NMR (400 MHz, DMSO) δ 11.01 (s, 1H), 8.41 (d, J = 8.4 Hz, 1H), 7.83–7.78 (m, 3H), 7.51–7.36 (m, 5H), 7.07 (dd, J = 8.4, 2.0 Hz, 1H), 6.91 (t, J = 5.6 Hz, 1H); ^{13}C-NMR (100 MHz, DMSO) δ 189.7, 168.5, 146.4, 144.6, 137.1, 135.1, 134.2, 131.1, 129.0, 128.9, 128.8, 128.2, 127.7, 121.5, 119.1, 110.3; ESI-MS: m/z 308.1 $[M - H]^-$.

(*Z*)-5-Bromo-3-((*E*)-2-oxo-4-phenylbut-3-en-1-ylidene)indolin-2-one (4w)

Red solid, yield 91%, m. p. 193–194 °C; ^{1}H-NMR (400 MHz, DMSO) δ 10.93 (s, 1H), 8.61 (d, J = 1.6 Hz, 1H), 7.94–7.74 (m, 3H), 7.55 (dd, J = 8.4, 2.0 Hz, 1H), 7.49–7.43 (m, 5H), 6.86 (d, J = 8.4 Hz, 1H); ^{13}C-NMR (100 MHz, DMSO) δ 189.7, 168.0, 144.9, 144.2, 135.3, 135.3, 134.3, 131.1, 129.7, 129.2, 129.0, 128.9, 127.6, 122.1, 113.2, 112.2; ESI-MS: m/z 352.1 $[M - H]^-$.

(*Z*)-5-Methyl-3-((*E*)-2-oxo-4-phenylbut-3-en-1-ylidene)indolin-2-one (4x)

Red solid, yield 81%, m. p. 169–170 °C; ^{1}H-NMR (400 MHz, DMSO) δ 10.67 (s, 1H), 8.24 (s, 1H), 7.86–7.77 (m, 3H), 7.50–7.45 (m, 3H), 7.41 (d, J = 14.8 Hz, 2H), 7.18 (dd, J = 8.0, 0.8 Hz, 1H), 6.78 (d, J = 8.0 Hz, 1H), 2.27 (s, 3H); ^{13}C-NMR (100 MHz, DMSO) δ 189.8, 168.5, 144.3, 142.8, 136.5, 134.3, 133.5, 130.9, 130.4, 129.0, 128.9, 127.8, 127.7, 127.6, 120.3, 109.9, 20.7; ESI-MS: m/z 288.1 $[M - H]^-$.

(*Z*)-1-Methyl-3-((*E*)-2-oxo-4-phenylbut-3-en-1-ylidene)indolin-2-one (4y)

Red solid, yield 90%, m. p. 114–115 °C; ^{1}H-NMR (400 MHz, DMSO) δ 8.30 (d, J = 7.6 Hz, 1H), 7.81–7.72 (m, 3H), 7.49–7.40 (m, 5H), 7.32 (d, J = 16.0 Hz, 1H), 7.03 (dd, J = 14.8, 7.6 Hz, 2H), 3.16 (s, 4H); ^{13}C-NMR (100 MHz, DMSO) δ 190.1, 167.2, 145.8, 144.9, 135.0, 134.1, 133.0, 131.2, 129.1, 128.9, 128.4, 127.4, 126.8, 122.4, 119.4, 109.1, 26.1; ESI-MS: m/z 290.3 $[M + H]^+$.

Anti-tumor assay

Briefly, targeted cancer cells lines (3×10^3 per well) were seeded in 96-well plates and cultured for 24 h, followed by compounds treatment for 48 h. A volume of 20 μL of 5 mg mL^{-1} MTT was added per well and incubated for another 2 h at 37 °C, then the supernatant fluid was removed and DMSO was added 150 μL per well for 15–20 min. The absorptions (OD) were measured at 570 nm with Spectra MAX M5 microplate spectrophotometer (Molecular Devices). The effect of compounds on tumor cells viability was expressed by IC_{50} of each cell line. Each assay was carried out at least three times. The results are summarized in Tables 1 and 2.

Docking simulation

The molecular docking method was used for the analysis of compound **4b** binding with Pim-1, Pim-2 and Pim-3. The GOLD docking program (version 5.0) was adopted here. The X-ray crystal structure of Pim-1 (PDB ID: 1XWS) was taken from PDB database, and the 3D structure of Pim-2 and Pim-3 were built using the homology modelling module in Discovery Studio 3.1. The preparation of protein structure, including adding hydrogen atoms, removing water molecules, and assigning

Charmm force field, were carried out by using Discovery Studio 3.1 software package. A sphere containing the residues in ATP binding pocket of protein structure were defined as the binding site. Goldscore was selected as the score function, and the other parameters were set as default. For each docking study, a total of 20 docking poses were retained. The root-mean square deviation (RMSD) between docking poses were calculated.

A reverse docking method was used for predicting the other possible kinase targets for compound **4b**. Detailed description of the reverse docking method please see ref. 40 (*Journal of Molecular Graphics and Modelling*, 2013, **44**, 278–285). Here the target database only includes top 10 kinases.

Hoechst staining

Briefly, cells (1×10^5 per well) were seeded in 6-well plates and cultured for 24 h, followed by **4b** treatment for another 48 h. After rinsing with PBS, the cells were fixed using 75% of ethanol. The morphological change of cell was examined by inverted microscope, then the cells were stained with Hoechst 33342 (2 lg mL^{-1}, in PBS) and analyzed under fluorescence microscope (Zeiss, Axiovert 200, Germany) to identify the apoptotic cells.

Cell-cycle distribution by flow cytometry

Briefly, cells were seeded in 6-well plates at the density of (1×10^5 per well) and cultured for 24 h, followed by compound **4b** treatment for another 48 h. At the indicated intervals, both attached cells and floating cells were harvested, sediments were resuspended in 1 mL hypotonic fluorochrome solution containing 50 μg mL^{-1} PI in 0.1% sodium citrate plus 0.1% Triton X-100, and then analyzed by flow cytometer (ESP Elite, Beckman-Coulter, Miami, FL). Cell cycle distribution was estimated with Listmode software.

Flow cytometric analysis of apoptosis

For Annexin V/PI assays, HeLa cells were stained with Annexin V-FITC and PI and then monitored for apoptosis by flow cytometry. Briefly, 5×10^3 cells were seeded in 6-well plates for 24 hours and then were treated with compound **4b** (0–8 μM) for 48 hours. Then cells were collected and washed twice with PBS and stained with 5 μL of Annexin V-FITC and 2.5 μL of PI (5 μg mL^{-1}) in 1 × binding buffer (10 mM HEPES, pH 7.4, 140 mM NaOH, 2.5 mM $CaCl_2$) for 30 minutes at room temperature in the dark. Apoptotic cells were quantified using a FACS can cytofluorometer. Statistical analysis was done using Flowjo 7.6.1 software. Both early apoptotic (Annexin V-positive, PI-negative) and late apoptotic (double positive of Annexin V and PI) cells were detected.

Immunohistochemistry of tubulin

HeLa cells were seeded on glass cover slips, incubated for 48 h in the presence or absence of test compound **4b**. Following the termination of incubation, cells were fixed with 3% formaldehyde, 0.02% glutaraldehyde in PBS and permeabilized by dipping the cells in 100% methanol (−20 °C). Later, cover slips were blocked with 1% BSA in phosphate buffered saline for 1 h followed by incubation with a primary anti-tubulin (mouse monoclonal) antibody and FITC conjugated secondary mouse anti IgG antibody. Photographs were taken using the confocal microscope, equipped with FITC settings and the pictures were analyzed for the integrity of microtubule network.

Conclusions

In conclusion, we have designed and synthesized a new series C3-functionalized oxindoles, 3-(2-oxo-4-phenylbut-3-en-1-ylidene)indolin-2-ones, and evaluated their anti-cancer activities against three cancer cell lines. Most of these compounds exhibited pronounced anti-tumor with IC_{50} values ranging from 0.03 to 17.32 μM. The most potent compound **4b** displayed remarkable inhibitory activities against a panel of different types of human cancer cell lines with IC_{50} values in the low micromolar range and showed much stronger effect than Cisplatin, as a positive control, on each cell line. The inhibition of Pim-1 and the molecular docking to Pim-1, suggested that compound **4b** was a potential Pim-1 inhibitor. Furthermore, flow cytometry (FCM), Hoechst 33342 staining assay and immunohistochemistry of tubulin indicated that compound **4b** induces cell death by apoptosis and compound **4b** leads to apoptotic cell death by inhibition of tubulin polymerization and influencing cell division, which were accordant to the biological phenomena resulted from the inhibition of Pim-1. Based on these results, it's evident that the novel series of 3-(2-oxo-4-phenylbut-3-en-1-ylidene)indolin-2-ones, particularly compound **4b**, have the potential to be developed as a new class of inhibitors of Pim-1 with efficient anti-cancer activity by further structural modifications. Further study on the anti-tumor activities *in vivo* and exact biological mechanism is underway.

Acknowledgements

We appreciate the financial support of National Natural Science Foundation of China (no. 81202403). We also thank Sichuan University Analytical & Testing Center for the NMR analysis.

Notes and references

1 T. Mochizuki, C. Kitanaka, K. Noguchi, T. Muramatsu, A. Asai and Y. Kuchino, *J. Biol. Chem.*, 1999, **274**, 18659–18666.
2 M. Bachmann, C. Kosan, P. X. Xing, M. Montenarh, I. Hoffmann and T. Möröy, *Int. J. Biochem. Cell Biol.*, 2006, **38**, 430–443.
3 T. L. Aho, J. Sandholm, K. J. Peltola, H. P. Mankonen, M. Lilly and P. J. Koskinen, *FEBS Lett.*, 2004, **571**, 43–49.
4 J. J. Gu, Z. Wang, R. Reeves and N. S. Magnuson, *Oncogene*, 2009, **28**, 4261–4271.
5 B. Nandini, Z. P. Wang, C. Davitt, I. F. C. Mckenzie, P. X. Xing and N. S. Magnuson, *Chromosoma*, 2002, **111**, 80–95.
6 R. Amson, F. Sigaux, S. Przedborski, G. Flandrin, D. Givol and A. Telerman, *Proc. Natl. Acad. Sci. U. S. A.*, 1989, **86**, 8857–8861.

7 E. D. Hsi, S. H. Jung, R. Lai, J. L. Johnson, J. R. Cook, D. Jones, S. Devos, B. D. Cheson, L. E. Damon and J. Said, *Leuk. Lymphoma*, 2008, **49**, 2081–2090.
8 S. J. Guo, X. P. Mao, J. X. Chen, B. Huang, C. Jin, Z. B. Xu and S. P. Qiu, *J. Exp. Clin. Cancer Res.*, 2010, **29**, 161.
9 S. M. Dhanasekaran, T. R. Barrette, D. Ghosh, R. Shah, S. Varambally, K. Kurachi, K. J. Pienta, M. A. Rubin and A. M. Chinnaiyan, *Nature*, 2001, **412**, 822–826.
10 B. Yan, E. X. Yau, S. Samanta, C. W. Ong, K. J. Yong, L. K. Ng, B. Bhattacharya, K. H. Lim, R. Soong, K. G. Yeoh, N. Deng, P. Tan, Y. L. Lam and M. Salto-Tellez, *Gastric Cancer*, 2012, **15**, 188–197.
11 C. Blanco-Aparicio and A. Carnero, *Biochem. Pharmacol.*, 2013, **85**, 629–643.
12 M. Bachmann, H. Hennemann, P. X. Xing, I. Hoffmann and T. Möröy, *J. Biol. Chem.*, 2004, **279**, 48319–48328.
13 L. S. Chen, S. Redkar, P. Taverna, J. E. Cortes and V. Gandhi, *Blood*, 2011, **118**, 693–702.
14 Z. Xia, C. Knaak, J. Ma, Z. M. Beharry, C. McInnes, W. X. Wang, A. S. Kraft and C. D. Smith, *J. Med. Chem.*, 2009, **52**, 74–86.
15 N. M. Santio, R. L. Vahakoski, E. M. Rainio, J. A. Sandholm, S. S. Virtanen, M. Prudhomme, F. Anizon, P. Moreau and P. J. Koskinen, *Mol. Cancer*, 2010, **9**, 279–291.
16 V. Pogacic, A. N. Bullock, O. Fedorov, P. Filippakopoulos, C. Gasser, A. Biondi, S. Meyer-Monard, S. Knapp and J. Schwaller, *Cancer Res.*, 2007, **67**, 6916–6924.
17 M. Haddach, J. Michaux, M. K. Schwaebe, F. Pierre, S. E. O'Brien, C. Borsan, J. Tran, N. Raffaele, S. Ravula, D. Drygin, A. Siddiqui-Jain, L. Darjania, R. Stansfield, C. Proffitt, D. Macalino, N. Streiner, J. Bliesath, M. Omori, J. P. Whitten, K. Anderes, W. G. Rice and D. M. Ryckman, *ACS Med. Chem. Lett.*, 2012, **3**, 135–139.
18 H. Nakano, N. Saito, L. Parker, Y. Tada, M. Abe, K. Tsuganezawa, S. Yokoyama, A. Tanaka, H. Kojima, T. Okabe and T. Nagano, *J. Med. Chem.*, 2012, **55**, 5151–5164.
19 S. Peddibhotla, *Curr. Bioact. Compd.*, 2009, **5**, 20–38.
20 D. J. Faulkner, *Nat. Prod. Rep.*, 2001, **18**, 1–49.
21 I. Ninomiya, *J. Nat. Prod.*, 1992, **55**, 541–564.
22 F. Zhou, Y. L. Liu and J. Zhou, *Adv. Synth. Catal.*, 2010, **352**, 1381–1407.
23 A. K. Franz, P. D. Dreyfuss and S. L. Schreiber, *J. Am. Chem. Soc.*, 2007, **129**, 1020–1021.
24 S. R. Yong, A. T. Ung, S. G. Pyne, B. W. Skeltonb and A. H. White, *Tetrahedron*, 2007, **63**, 5579–5586.
25 Raunak, V. Kumar, S. Mukherjee, Poonam, A. K. Prasad, C. E. Olsen, S. J. C. Schäffer, S. K. Sharma, A. C. Watterson, W. Erringtone and V. S. Parmar, *Tetrahedron*, 2005, **61**, 5687–5697.
26 V. Sharma, S. Peddibhotla and J. J. Tepe, *J. Am. Chem. Soc.*, 2006, **128**, 9137–9143.
27 M. Kitajima, I. Mori, K. Arai, N. Kogure and H. Takayama, *Tetrahedron Lett.*, 2006, **47**, 3199–3202.
28 Y. Kamano, H. P. Zhang, Y. Ichihara, H. Kizu, K. Komiyama and G. R. Pettit, *Tetrahedron Lett.*, 1995, **36**, 2783–2784.
29 H. Suzuki, H. Morita, M. Shiro and J. Kobayashi, *Tetrahedron*, 2004, **60**, 2489–2495.
30 Y. Q. Tang, I. Sattler, R. Thiericke, S. Grabley and X. Z. Feng, *Eur. J. Org. Chem.*, 2001, **2001**, 261–267.
31 Y. L. Hsu, P. L. Kuo, W. S. Tzeng and C. C. Lin, *Food Chem. Toxicol.*, 2006, **44**, 704–713.
32 M. M. Rafi, R. T. Rosen, A. Vassil, C. T. Ho, H. Zhang, G. Ghai, G. Lambert and R. S. Dipaola, *Anticancer Res.*, 2000, **20**, 2653–2658.
33 S. Yamazaki, T. Morita, H. Endo, T. Hamamoto, M. Baba, Y. Joichi, S. Kaneko, Y. Okada, T. Okuyama, H. Nishino and A. Tokue, *Cancer Lett.*, 2002, **183**, 23–30.
34 Y. L. Hsu, P. L. Kuo and C. C. Lin, *Life Sci.*, 2005, **77**, 279–292.
35 Y. Wang, F. L. Chan, S. Chen and L. K. Leung, *Life Sci.*, 2005, **77**, 39–51.
36 A. Jemal, R. Siegel, J. Xu and E. Ward, *Ca-Cancer J. Clin.*, 2010, **60**, 277–300.
37 J. K. Buolamwini, *Curr. Opin. Chem. Biol.*, 1999, **77**, 500–509.
38 J. Liu, H. B. Sun, X. J. Liu, L. Ouyang, T. R. Kang, Y. M. Xie and X. Y. Wang, *Tetrahedron Lett.*, 2012, **53**, 2336–2340.
39 T. T. Yan, X. Y. Wang, H. B. Sun, J. Liu and Y. M. Xie, *Molecules*, 2013, **18**, 14505–14518.
40 G. B. Li, L. L. Yang, Y. Xu, W. J. Wang, L. L. Li and S. Y. Yang, *J. Mol. Graph. Model.*, 2013, **44**, 278–285.

